

Generalized Local-to-Global Shape Feature Detection Based on Graph Wavelets

Nannan Li, Shengfa Wang, Ming Zhong, Zhixun Su, and Hong Qin, *Senior Member, IEEE*

Abstract—Informative and discriminative feature descriptors are vital in qualitative and quantitative shape analysis for a large variety of graphics applications. Conventional feature descriptors primarily concentrate on discontinuity of certain differential attributes at different orders that naturally give rise to their discriminative power in depicting point, line, small patch features, etc. This paper seeks novel strategies to define generalized, user-specified features anywhere on shapes. Our new region-based feature descriptors are constructed primarily with the powerful spectral graph wavelets (SGWs) that are both multi-scale and multi-level in nature, incorporating both local (differential) and global (integral) information. To our best knowledge, this is the first attempt to organize SGWs in a hierarchical way and unite them with the bi-harmonic diffusion field towards quantitative region-based shape analysis. Furthermore, we develop a local-to-global shape feature detection framework to facilitate a host of graphics applications, including partial matching without point-wise correspondence, coarse-to-fine recognition, model recognition, etc. Through the extensive experiments and comprehensive comparisons with the state-of-the-art, our framework has exhibited many attractive advantages such as being geometry-aware, robust, discriminative, isometry-invariant, etc.

Index Terms—Shape feature detection, spectral graph wavelets, bi-harmonic field, region descriptor, partial matching

1 INTRODUCTION

STUDIES in feature abstraction and analysis have been gaining momentum because they can assist numerous downstream graphics tasks and applications such as shape recognition, segmentation, analysis, understanding, etc. [1], [2], [3]. Influenced by the newly-arisen concept of high-level representations in computer vision, which are based on object-wise components, now much more attention has been directed towards region-wise feature analysis in computer graphics. In this paper, we advocate a new region-based and user-specified type of feature as well as a novel graph-wavelet-inspired multi-scale and multi-level descriptor, and they jointly enable our feature detection framework that can further facilitate various practical applications.

Conventional feature descriptors are usually constructed by considering the discontinuities of certain differential attributes at different orders (e.g., the second-order attribute like surface curvature) that naturally afford their discriminative power in characterizing point features, line/curve features, small patch-based features with regular boundaries, etc. Such descriptions have facilitated

point/patch-based recognition, point-wise correspondence, and curvature-based saliency detection with great success. However, for more complex applications such as modeling by example [4], model composition [5], and key component analysis [6], the aforementioned conventional features are usually too localized to capture the multi-scale neighboring information, and it is desirable to have a flexible, region-wise feature description. Furthermore, in many real-world settings, shape data may be degraded due to acquisition imperfections and noises, necessitating the use of region descriptors which tend to be much more robust.

Existing works related to region-wise analysis include partial matching, shape correspondence, saliency extraction, etc. Boundaries of the regions in question are usually confined to regular but non-adaptive shapes [7], [8], [9], [10], thus neighboring and in-between geometry information may not be fully captured. As for region description, trending measures include the distributions of various types of point descriptors [11], [12], [13] and the global analysis of the regions based on spectral decomposition [14], [15]. Some regional measures are not discriminative enough to solely characterize the regions in question, for which post-processing like geometric hashing [16] or random sample consensus [17] is required. Nevertheless, these settings are not hierarchical enough to characterize the focal regions. On the other hand, multi-scale shape analysis methods [18], [19], in spite of their great descriptive power, have not yet been employed to construct regional descriptions. These insights inspire us to propose a more comprehensive and stable type of shape description that can encode the region of interest with high discriminative power and efficiency.

In this paper, we propose a local-to-global shape feature via user specification, introduce an informative region descriptor, and then present a shape feature detection framework to facilitate a host of graphics applications. The

- N. Li is with the School of Mathematical Sciences, Dalian University of Technology, Dalian, Liaoning, China. E-mail: nannanli2013@gmail.com.
- S. Wang is with the School of Software Technology and Key Laboratory for Ubiquitous Network and Service Software of Liaoning Province, Dalian University of Technology. E-mail: sfwang@dlut.edu.cn.
- M. Zhong and H. Qin are with the Department of Computer Science, Stony Brook University, NY. E-mail: {mzhong, qin}@cs.stonybrook.edu.
- Z. Su is with the School of Mathematical Sciences, Dalian University of Technology and National Engineering Research Center of Digital Life, Dalian, Liaoning, China. E-mail: zxsu@dlut.edu.cn.

Manuscript received 25 Sept. 2014; revised 3 Oct. 2015; accepted 29 Oct. 2015. Date of publication 6 Nov. 2015; date of current version 3 Aug. 2016.

Recommended for acceptance by A. Sheffer.

For information on obtaining reprints of this article, please send e-mail to: reprints@ieee.org, and reference the Digital Object Identifier below.

Digital Object Identifier no. 10.1109/TVCG.2015.2498557

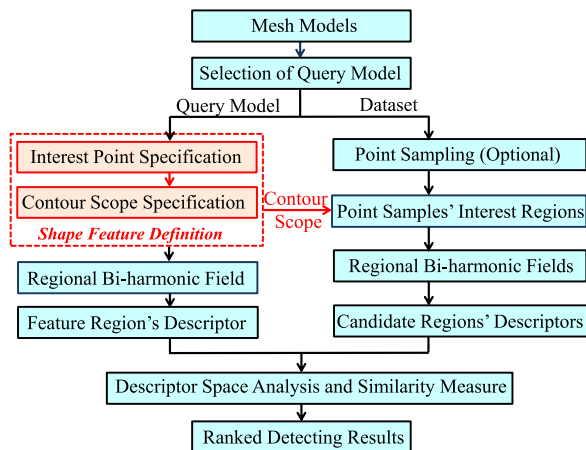


Fig. 1. The pipeline of our approach.

proposed shape feature extends the definition of conventional features to a region-wise manner in a user-specified way (as highlighted in Fig. 1). To encode user-specified features, we proactively seek an informative regional descriptor constructed in a multi-scale and multi-level way. Our descriptor takes advantage of the bi-harmonic distance field and the SGWs. The stability and robustness of bi-harmonic distance field guarantee the technically-sound foundation for the whole descriptor. SGWs naturally accommodate local and global geometry with a multi-scale solution, and such solution is consistent across multiple levels. We devise a new statistical method based on the decomposition coefficients of the shape signal, enabling the joint analysis of the underlying geometry together with different shape signals. In order to comprehensively characterize the shape features, we also incorporate the contour-centered geometric statistics into our descriptor. All of these enable our feature detection framework as shown in Fig. 1. We quantify each model's regions of interest around central points (or point samples) according to the user-specified feature scope on the query model. Then descriptors are constructed on candidate regions across different models, which is equivalent to transform each region into the high-dimensional feature space. After the region-wise feature space is constructed, various analytical tasks can be performed. The primary contributions of this paper can be summarized as follows:

- We propose to define a generalized shape feature type via user specification, which is geometry-aware and is the organic coupling of local and global description. Also, it is a fundamental tool that can help unite different types of graphics applications.
- Our region-based descriptor is primarily built upon the SGWs that are both multi-scale and multi-level in nature, elegantly integrating both local (differential) and global (integral) information. We also introduce the contour-centered geometric statistics to enhance the descriptor's discriminative power.
- We develop a feature detection framework, which can integrate different types of state-of-the-art region descriptors and further facilitate widespread graphics applications including partial matching, coarse-to-fine recognition, model recognition, etc.

2 RELATED WORK AND BACKGROUND REVIEW

This section will briefly review prior research related to region analysis and the latest progresses on SGWs.

Region-wise description and detection. We first review how current methods define boundaries for given regions. Broadly speaking, they characterize a local neighborhood around a central point in two ways. The first is based on Euclidean distance, such as spheres [7], blowing bubbles [8], rings [9], shape context [10] or priori decompositions [20], [21]. The second is to use geodesic distance like geodesic fans [22] and spiral pathway [23]. The shapes of region boundaries defined by the above methods are mostly restricted to regular formats, and such nonadaptive neighborhoods cannot precisely reflect the local geometrical or topological distortions. Region-wise descriptors can be roughly divided into two categories: point-based and region-based methods. Point-based methods provide the quantitative measure by organizing single-valued point signatures into certain kinds of distributions. Various kinds of point descriptors have been incorporated in this manner, e.g., the shape index (SI) [24], shape diameter function (SDF) [25], heat kernel signature (HKS) [26], Zernike moments [27], etc. Region-based methods analyze the entire focal region through spectral decomposition [14], [28], which can robustly depict the intrinsic geometry. However, due to the instability of local Laplacian decomposition, these methods usually cannot well handle small and complex regions.

Region-based partial matching and correspondence. In literature, region analysis has been discussed mainly in the research of partial matching problems, and several categories of techniques have been employed. Skeletal-graph-based approaches such as [29] couple geometry and structure in a single skeletal descriptor based on the theory of Reeb graph. The main drawback is that sub-parts cannot be recognized automatically. Multi-criterion optimization approaches [23], [30], [31] try to match subparts by striking balance between significance and similarity criteria. This type of methods require the knowledge of correspondence between shapes, otherwise, it can only be solved by alternating between correspondence and part area, which is time-consuming. Bag-of-words (BoWs) technique has been adopted [32], [33] to represent a shape or a subpart as a collection of local feature signatures quantized in some vocabularies of "geometric words". If the geometric vocabulary is sufficient and the shapes have significant common parts, it is possible to compare partially-similar shapes, otherwise, these methods oftentimes fail to function properly. Furthermore, improper additions of the spatial information and imprecise binning process may lead to the averaging-off effects of geometric information. The concept of non-point-wise correspondence was first proposed in [26] by using region-wise local descriptors and optimizing over the integration domain upon which the integral descriptors of the two parts match. This method can exactly match fragments to entire shapes, however, since it utilizes the absolute values in calculation like integration, it cannot deal with the partially similar correspondence. Besides, many of the above approaches rely heavily on exact or meaningful shape decomposition process as in [15], [21], which is computationally expensive and significantly influences the final

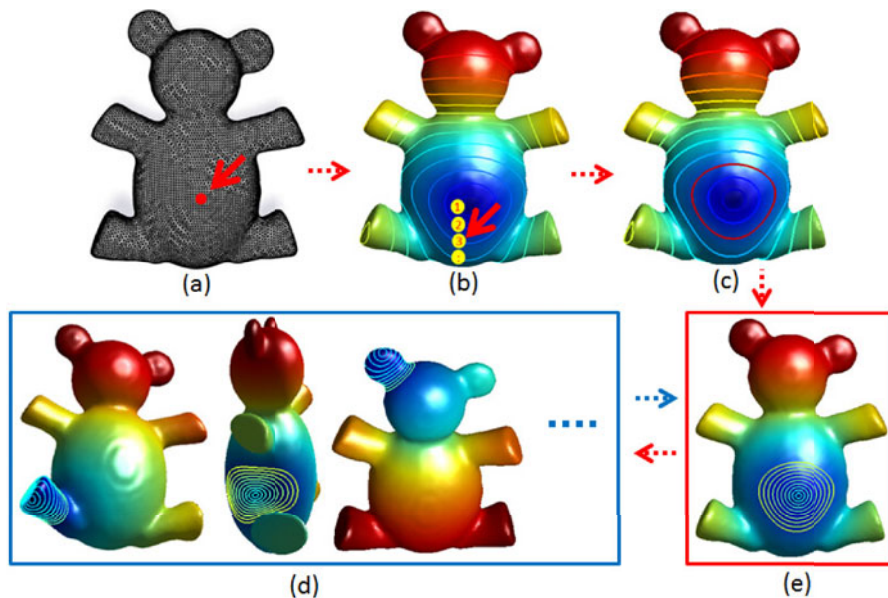


Fig. 2. The functional pipeline of our feature detection framework. (a)-(c) show the user's inputs in the specification process, red arrows in (a) and (b) denote the specified point of interest and contour scope, respectively. The bottom row shows the specified shape feature (e) and analogous feature regions (d) (we only display three cases here).

correspondence results. Also, in order to achieve meaningful results, many approaches utilize time-consuming post-processing like in [20] and [21]. So it requires more effective and generalized region detection techniques to help speed up and improve the precision of the partial matching and correspondence processes.

Spectral graph wavelets. Wavelet, which can localize a given function both in space and in scale, is a powerful analytical tool in signal processing [34]. Unlike Fourier transform which are globally defined, wavelet analysis is able to perform localized multi-resolution analysis. Classical wavelets are constructed by translating and scaling a mother wavelet in Euclidean space. However, transplanting wavelets to graphs (specifically, triangular meshes) is not straightforward due in part to the fact that it is unclear how to apply the scaling operation on a signal that is defined on the mesh vertices, so early studies using wavelet mostly relied on the parameterization [35], [36]. One way to construct wavelets on graph structures is using a diffusion operator and its dyadic powers to obtain multi-scale wavelet and scaling functions [37], [38]. Another approach to define graph wavelets is by expanding graph functions with the eigen-system of the graph Laplacian matrix and performing scaling in the frequency domain [39], [40], giving rise to the spectral graph wavelet transform (SGWT). More recently, Kim et al. [41], [42] introduced a wavelet-based multi-scale descriptor for the analysis of cortical surface signals using the SGWT and Li et al. [43] proposed a SGWT-based descriptor and utilized the intrinsic spatial pyramid matching (ISPM) for global shape retrieval. Though these researches discover the potentials of SGWs, they all concentrate on global shape analysis based on point signatures, ignoring the SGWs' power in integrating the local-to-global/in-between geometrical and topological information. These inspire us to combine SGWs and bi-harmonic distance field to enable the multi-scale and multi-level description of the region of interests.

3 LOCAL-TO-GLOBAL SHAPE FEATURE DEFINITION

In this section, we introduce the definition process of the proposed novel shape feature, which generalizes conventional features (e.g., point, line, or patch features) to a local-to-global level via user specification. Our shape feature is extracted via the bi-harmonic distance field [44], which is robust, globally "shape-aware", parameter-free, and widely used in geometry processing. Among these attractive properties, the consecutive depicting power inspires us to incorporate it for integrating multi-scale regional information that is required for subsequent analysis. In addition, the cross-sections of contours in the bi-harmonic distance field naturally form boundaries for user-specified features, thus avoiding the shape decomposition process.

Our shape feature is a user-specified partial region with two parameters: the point of interest and the contour scope, both of which can be determined using a simple user-interactive process. The point of interest is the relative center of the feature, it can either be picked directly on the mesh, as shown in Fig. 2a, or be automatically initialized as the extreme point of a function defined on the surface. In order to specify the contour scope of the point of interest, we should first introduce the metric with which we set the scope, namely, the bi-harmonic distance field.

Let us consider a 3D mesh represented as a graph $M = (V; E)$ with vertices V and edges E , where $V = \{v_1, v_2, \dots, v_n\}$ and n is the number of the vertices. A vector-valued function $f: V \rightarrow \mathbb{R}^q$ defined on V can be represented as an $n \times q$ matrix, where the i th row represents the function value at v_i , we denote it as $f(i)$. According to [44], the bi-harmonic distance between vertex v_i and v_j can be expressed as

$$D_{bh}(i, j)^2 = \sum_{k=1}^m \frac{(\chi_k(i) - \chi_k(j))^2}{\lambda_k^2}, \quad (1)$$

where $\{\lambda_k\}$ and $\{\chi_k(\cdot)\}$ are, respectively, the first m non-zero eigenvalues and the corresponding eigenfunctions of the Laplacian-Beltrami operator with ‘‘cotangent formula’’ discretization [45].

For each vertex, Eq. (1) defines a diffusion field around it. We compute the diffusion field of the specified interest point (denoted as v_s) and then construct a set of contours (Fig. 2b) across the entire model with contour points located on the edges of the mesh model. These contours can very well reflect the changes locally around the central point and characterize the corresponding global structures, and these will be discussed later. In order to make the setting of parameters more stable, we normalize the original models using a unit box. Then the total number of the contours distributed in the diffusion field can be set empirically to the integer nearest to $\max(D_{bh}(s, \cdot))/0.05$, which is dense enough to depict the diffusion field. Then the user can choose one of the contours to set the scope of the feature (as shown in Fig. 2b) and denote it as S_s . Fig. 2c illustrates the feature defined with the red boundary.

Our shape features can be located anywhere and vary spatially in scale depending on specific applications. They integrate the local and global geometry, which affords their great potential in bridging differential and integral geometry information.

4 MULTI-LEVEL AND MULTI-SCALE SHAPE DESCRIPTION

Our novel descriptor primarily exploits the SGWs and the metric statistics. This section introduces the SGWs-related description and the contour-based statistics before the complete descriptor can be constructed.

4.1 SGW-Based Description

SGWT is introduced in [39] to conduct wavelet analysis on graphs. The core idea is to define the required scaling in the Fourier domain instead of the spatial domain. SGWT is determined by the generating kernel $g: \mathbb{R} \rightarrow \mathbb{R}$. To act as a band-pass filter, the kernel g should satisfy $g(0) = 0$ and $\lim_{x \rightarrow \infty} g(x) = 0$. SGWs, as described in [39], are expressed as bivariate kernel functions expanded on the manifold harmonic basis, which are formed by the aforementioned Laplacian-Beltrami eigenfunctions on mesh models

$$\Psi_t(i, j) = \sum_{k=0}^{n-1} g(t\lambda_k) \chi_k(i) \chi_k(j), \quad (2)$$

where g is the real-valued SGWs generating kernel and t is the scale parameter. The i -th row of $\Psi_t(\cdot, \cdot)$

$$\psi_{t,i}(\cdot) = \Psi_t(i, \cdot) = \sum_{k=0}^{n-1} g(t\lambda_k) \chi_k(i) \chi_k(\cdot), \quad (3)$$

is the spectral wavelet spatially-localized at v_i , and in the frequency domain, localized at scale t . Fig. 3 shows the SGWs of different scales located on one index point on the wolf model. It may be noted that, the values of wavelets are attenuated and oscillating on the mesh, and wavelets with a larger scale have a wider oscillating window. Here it should be emphasized that we choose to utilize the geometric

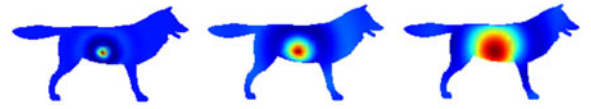


Fig. 3. Spectral Graph Wavelets centered at one vertex on the wolf model. From left to right are wavelets from high frequency to low frequency with scale 1, 3 and 5.

mesh Laplacian instead of the combinatorial Laplacian as originally applied in [39] to afford much more precise description of the mesh geometry.

It has been proved that SGWs can well represent the high frequency and low frequency geometric information around the index point [39]. Suppose we compute the spectral wavelets at J different scales $\{t_1, t_2, \dots, t_J\}$, and adopt the same formulation of generating kernel functions used in [39], given by

$$g(x) = \begin{cases} x^2 & \text{if } x < 1 \\ -5 + 11x - 6x^2 + x^3 & \text{if } 1 \leq x \leq 2, \\ 4x^{-2} & \text{if } x > 2 \end{cases}, \quad (4)$$

and the J scales are selected to be logarithmically equally spaced between the minimum scale $t_J = 2/\lambda_{max}$ and the maximum scale $t_1 = 40/\lambda_{max}$, where λ_{max} is the upper bound of the Laplacian eigenvalues. The settings of t_1 and t_J guarantee that $g(t_1x)$ has power-law decay for $x > \lambda_{min}$ and $g(t_Jx)$ has monotonic polynomial behavior for $x < \lambda_{max}$.

Using the above formulations, we can easily get the wavelet coefficients of a given function on a specific vertex v_i as

$$W_f(t, i) = \langle \psi_{t,i}, f \rangle = \sum_{l=0}^{n-1} g(t\lambda_l) \hat{f}(l) \chi_l(i), \quad (5)$$

where

$$\hat{f}(l) = \langle \chi_l, f \rangle = \sum_{i=0}^{n-1} \chi_l(i) f(i), \quad (6)$$

and

$$f(i) = \sum_{l=0}^{n-1} \hat{f}(l) \chi_l(i). \quad (7)$$

Here, the signal function f can be any kind of surface signal depending on applications. For example, mean curvature, characterizing detailed distortions, is a good choice for the recognition of repetitive features within certain models, the detection of similar features among models with different poses, etc. For coarse-to-fine recognition, the HKS is more favorable thanks to its robustness to noise. Different settings of f will be shown throughout our paper in various applications. The coefficients W_f obtained from the transformation is the inner product of the signal function and the corresponding wavelet at scale t and location i . It is a representation of the signal for that scale, that is to say, it describes the original signal in certain frequency with respect to the local geometry and topology. Repeating this process for J scales (as shown in Figs. 4a, 4b, 4c, and 4d with four scales), the set of coefficients obtained comprises our multi-level descriptor.

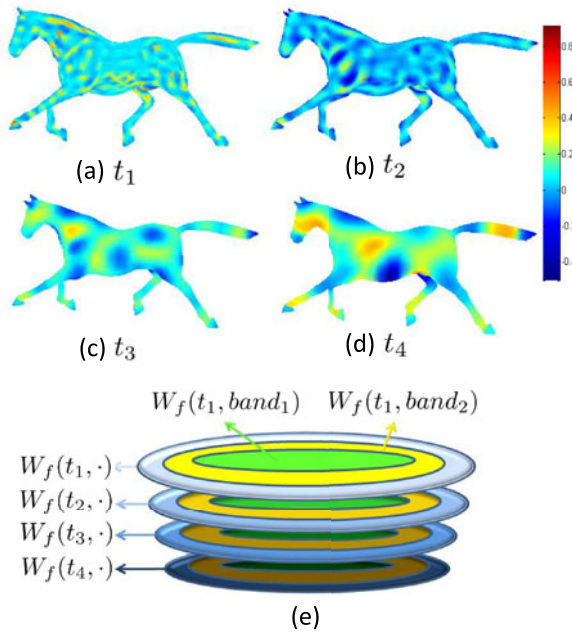


Fig. 4. Statistics on signal's wavelet decomposition coefficients ($W_f(\cdot, t)$). (a)-(d) list t from small (t_1) to large (t_4) value, corresponding to the decomposed signals varying from high to low frequencies. (e) illustrates the composition of statistics based on W_f within one feature region.

Instead of using W_f directly as the descriptor like in [43] and other harmonic analysis researches, we incorporate it into our descriptor by taking advantage of the consecutive depicting power of the bi-harmonic distance field. In order to comprehensively describe the geometric information contained within the feature, we subdivide the feature region into thinner bands with more contours as implemented in Section 3, just as shown in Figs. 2c, 2d, and 2e. The number of dense contours may be set automatically as the integer nearest to $S_s/0.025$, and such dense contours have been verified to be able to elaborately depict and organize the inner geometrical information of the feature. Fig. 4e illustrates the setup of our SGW-based statistical bands based on W_f , where different layers convey multi-level (from high to low frequency) information and different bands (denoted in yellow and green) in-between contours encode multi-scale information. By stretching the “matrix-like” statistic (as in Fig. 4e) into a high dimensional vector, we obtain the descriptor of v_s , denoted as D_s , given by

$$D_s = [W_{t_1}^{b_1}, \dots, W_{t_1}^{b_L}, W_{t_2}^{b_1}, \dots, W_{t_2}^{b_L}, \dots, W_{t_j}^{b_1}, \dots, W_{t_j}^{b_L}], \quad (8)$$

where $W_{t_i}^{b_j}$ denotes the statistic of W_f with scale t_i on the j th band, and L is the number of contours. Here $W_{t_i}^{b_j}$ can be expressed as the 1-norm of $W_f(t_i, \cdot)$ over the j th band

$$W_{t_i}^{b_j} = \sum_{p \in b_j} |W_f(t_i, p)|, \quad (9)$$

where p is the vertex index, $p \in b_j$ denotes p is a vertex located on the j th band.

In Fig. 4, we observe that information contained in W_f of different time scales corresponds to the fine-to-coarse multi-level information, and the statistics on the bands convey the

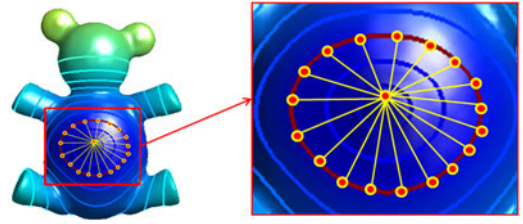


Fig. 5. Contour-based distance distribution. The zoomed-in part shows the distances under current consideration when performing statistical calculation.

near-to-far multi-scale knowledge. These collectively make use of SGWs' power in integrating geometric information. In addition, we notice that descriptors based on W_f are scale-invariant as long as SGWs are normalized.

4.2 Contour-Based Multi-Scale Statistics

The contours of bi-harmonic distance field encode rich information of local-to-global geometric variation. So we further introduce the perimeters of contours and the distance distribution of contour points to help characterize the focal region's shape in an orderly and quantitative manner.

For a specified feature and its corresponding contours, we first calculate contours' perimeters and concatenate them as $\{p^{c_1}, p^{c_2}, \dots, p^{c_L}\}$, where c_i denotes the index of the i -th contour. Then, for each contour, we compute the Euclidean distances between the contour points and their barycenter (as shown in Fig. 5), and further evaluate the probability distribution of the distances. We denote the distance-related statistics as $\{ds^{c_1}, ds^{c_2}, \dots, ds^{c_L}\}$. Here, ds^{c_i} is a vector stacking up the probability distribution of the distances concerning the i th contour. We uniformly separate the distance values into M bins, ranging from zero to the maximum value after removing the top and bottom 5 percent to rule out possible outliers. Then its stack pattern is

$$ds^{c_i} = \left[\frac{\text{num}(b_1)}{\text{num}(c_i)}, \frac{\text{num}(b_2)}{\text{num}(c_i)}, \dots, \frac{\text{num}(b_M)}{\text{num}(c_i)} \right], \quad (10)$$

where $\text{num}(b_j)$ is the number of points with distance values falling in the j th bin and $\text{num}(c_i)$ is the number of points on the i th contour. For multiple contours with the same value, they should be considered as a whole when performing statistical calculation.

These two measurements help describe the shape of the bi-harmonic distance field completely and identify the details of shape's distortion. The purpose of introducing the distance distribution is to distinguish between different contours with the same perimeters.

4.3 Informative Region-Based Descriptor

So far, the separate parts of our descriptor have all been introduced. Now, it sets the stage for us to integrate them together to form our final informative hi-dimensional descriptor as

$$D_s = [\omega_s * (W_{t_1}^{b_1}, \dots, W_{t_j}^{b_L}), \omega_p * (p^{c_1}, \dots, p^{c_L}), (ds^{c_1}, \dots, ds^{c_L})], \quad (11)$$

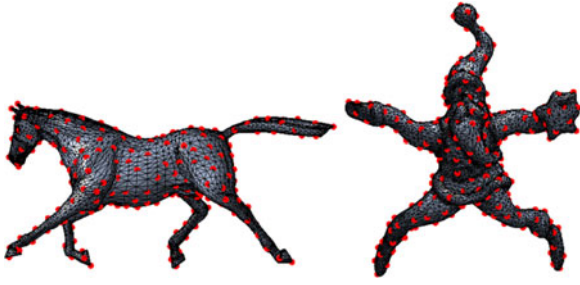


Fig. 6. Sampling results on horse and santa model using the farthest-point-sampling strategy. Only part of the sampling points are shown for visual clarity.

where ω_s and ω_p are weights to adjust the contributions of the three parts in the descriptor. The settings of these weights will be detailed in Section 6.

Our descriptor integrates the attractive properties of both SGWs and contour-based measurements. From the viewpoint of feature mapping, SGWs establish a powerful foundation for hierarchical representation of the geometrical and topological details. Our design of the regional description encodes the shape feature in the aspects of both “breadth” and “depth”, paving the way for our feature detection framework.

5 FEATURE DETECTION FRAMEWORK

Using the same way to define feature regions around candidate points and formulate the corresponding descriptions, descriptors concerning candidate regions on the same model or different models in the database can be easily computed for analytical purposes.

5.1 Constructing Descriptors over Shapes

To construct descriptors on candidate regions on one or more models, the central points and contour scopes should also be determined first. As for the central points, we implement the farthest-point-sampling strategy [46] to uniformly extract points on the mesh model (as shown in Fig. 6). This strategy ensures not only the uniform distribution of the candidate points, but also the inclusion of the end points, which are interesting alternatives for user’s selection. However, we want to mention that the sampling process is optional, and users could either pick the desired sampling methods or simply use all the vertices as candidates according to specific applications.

Then the construction of descriptors across versatile shapes is based on the knowledge of the shape feature defined. That is, candidate regions are determined automatically according to the contour scope of the shape feature specified. Suppose that v_s and v_i are respectively the interest point and one of the candidate points. Then the scope of v_i is set as $S_s * \max(D_{bh}(i, \cdot)) / \max(D_{bh}(s, \cdot))$ and this can help ensure the robustness of our method for deformable models. With the region scope determined, the construction of the corresponding descriptor is conducted in the same way as the specified feature (in Section 4), which is detailed in Algorithm 1.

With each candidate region equipped with a high-dimensional descriptor, our key task is to analyze the similarity in the descriptor space. We shall first introduce the proper measurements for this new space. It has been found

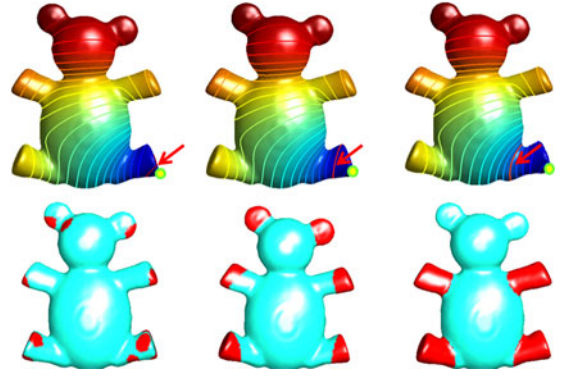


Fig. 7. Detection of repetitive features with different scales. The first row shows the specified features and the second row shows the detected results within the bear model. Yellow points on query models denote the specified points of interest.

that both $L1$ and $L2$ norms are discriminative enough to measure the distance between any two descriptors, representing the corresponding regions. As alternatives, the covariance distance and χ^2 distance are also tested to be good choices for comparing the distributions’ similarities.

Algorithm 1. Construction of Descriptors over Shapes

- Input:** User-specified interest point v_s and contour index n_s ;
Output: Descriptors of the specified feature (D_s) and all the other candidate regions ($\{D_i\}$);
- 1: Conduct the eigen-decomposition on all models;
 - 2: Compute the W_f of each point using Eq. (5);
 - 3: Compute the bi-harmonic distance of v_s , denoted as $D_{bh}\{s, \cdot\}$;
 - 4: Uniformly construct $\max(D_{bh}(s, \cdot)) / 0.05$ contours across the entire model;
 - 5: With user’s specification of the contour number (n_s), compute the corresponding value as S_s ;
 - 6: For any candidate point v_i , compute its bi-harmonic distance $D_{bh}\{s, \cdot\}$, and set its region scope as $S_s * \max(D_{bh}\{i, \cdot\}) / \max(D_{bh}\{s, \cdot\})$;
 - 7: Reconstruct $S_s / 0.025$ contours on the specified feature and all the candidate feature regions;
 - 8: Compute the SGWs-based and contour-related measurements using Eq. (11);
 - 9: Return D_s and $\{D_i\}$.
-

5.2 Feature Detection and Framework Properties

Here, we detail the effectiveness of our feature detection framework together with several of its attractive properties and more results will be shown in Section 6. It shall first be emphasized that high sampling rates always lead to dense distribution of the candidate points, thus several neighboring points may have similar diffusion regions, and this will lead to multiple detected results that are in the vicinity of each other. Therefore we empirically reject candidate regions that have more than 50 percent overlaying with the afore-ranked regions. This strategy can ensure the uniqueness of the detected features as well as the broader coverage of all relevant feature regions, and also make our approach robust to different sampling processes.

We first show a simple feature detection result within the bear model as displayed in Fig. 7 (here, mean curvature is chosen as the signal function). The top row shows the

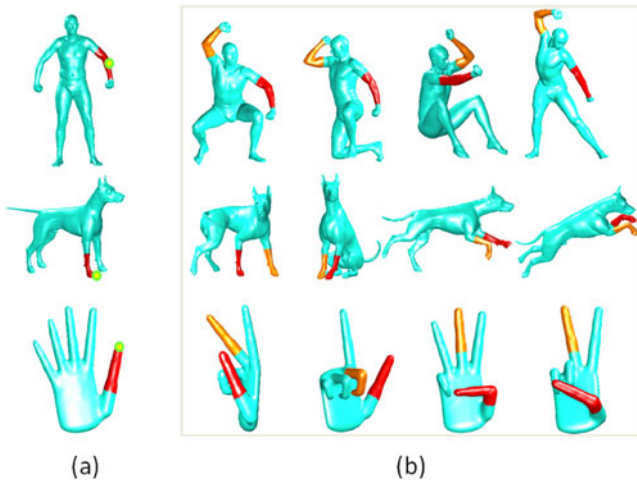


Fig. 8. Illustration of isometry-invariance. (a) Query. (b) Detected results on deformed models with red and orange denoting the top-2 similar regions.

features specified with different scales and the second row shows the detected results. It can be observed that the detected similar feature regions are affected by the specification of the feature scope (the selected contour indices here are 2, 3, and 6, respectively). Though small-scale query leads to rather trivial outcomes, the most similar parts are still among the top-ranked results. Furthermore, it is obvious that larger scales can lead to more accurate results thanks to added information. The analogous feature regions defined (proportional to the specified feature) and the corresponding descriptors jointly ensure the accuracy of the detection of the repetitive feature regions.

Our shape feature and its description possess many attractive properties like being concise to store, fast to compute, and efficient to match, etc. Here, we demonstrate two more desirable properties that can facilitate various practical tasks.

Isometry-invariance. We verify the property of isometry-invariance through tests carried on three categories of models in different poses. These models are chosen from the SCAPE and TOSCA databases. As visualized in Fig. 8, we deliberately specify features on the human arm containing the elbow, dog leg with elbow and finger with knuckle to validate the property. The models in Fig. 8b are the deformed ones showing the top-2 most similar feature regions detected on each of them (red and orange highlight the first and second one, respectively). The top-2 detected results are shown here since our approach is capable of identifying similar regions, but distinguishing between symmetric parts is beyond the technical scope of this paper. The retrieved results empirically prove that our region-based descriptor is isometry-invariant, which is inherited from the properties of graph wavelets and bi-harmonic distance field.

Robustness to noise. We add 0.5 (of the mesh’s mean edge length) noise to the query models as shown in Fig. 9a and set the signal as HKS. We selectively enlarge the SGWs-related part of our descriptor to combat noise. The features are specified on these noisy models as shown in Fig. 9b. From the detection results displayed in Fig. 9c, it can be observed that even with large noise, our approach can still

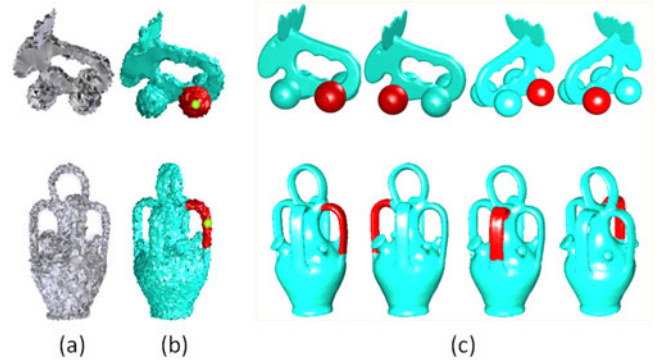


Fig. 9. Coarse-to-fine recognition on elk and kettle model with 0.5 (mean edge length) noise. (a) Noisy model. (b) Specified features. (c) Recognized regions.

recognize the intrinsic geometric characteristics of the features and identify the corresponding similar features, including the ball shape on the elk model and the bended handle of the kettle model from the shape database, thanks to the robustness and stability of bi-harmonic distance field and HKS. The robustness of our approach is of great significance in practical applications as will be demonstrated in Section 6.

6 EXPERIMENTAL RESULTS AND DISCUSSIONS

In this section, we demonstrate the performance of our approach via experiments in various aspects. All the experiments were conducted on a 3.5 GHz Intel(R) Core(TM) i7 computer with 16 GB memory. We used the cusparse and cublas libraries in CUDA to help reduce the computational time for wavelet transform significantly. For instance, for the SHREC 2007 partial retrieval dataset, in which the average model size is 18 K vertices, the whole process of constructing descriptors on one model takes an average of 0.38 minutes, and the whole database costs 114 minutes with 20 percent sampling rate for each model. More timing details concerning versatile models are shown in Table 1.

6.1 Parameter Evaluation

There are several parameters in our approach, most of them can be set automatically or empirically set as constants. Two parameters, the sampling rate and the signal function, could be tuned according to specific applications’ requirements for better results.

Parameters in the construction of descriptors. For the SGWs-related part of the descriptor, we calculate bi-harmonic distances and graph wavelets using the first 300 eigenvalues of each model, and they only need to be computed once. The

TABLE 1
Run Time for Constructing Descriptors

Model	# vertices	Timing (min)		
		Eigen	W_f	Total
Dinosaur	14K	0.17	0.14	0.33
Dog	26K	0.30	0.35	0.69
Armadillo	34K	0.38	0.48	0.97
Santa	75K	0.93	1.23	2.32
Dragon	430K	5.51	8.16	14.15

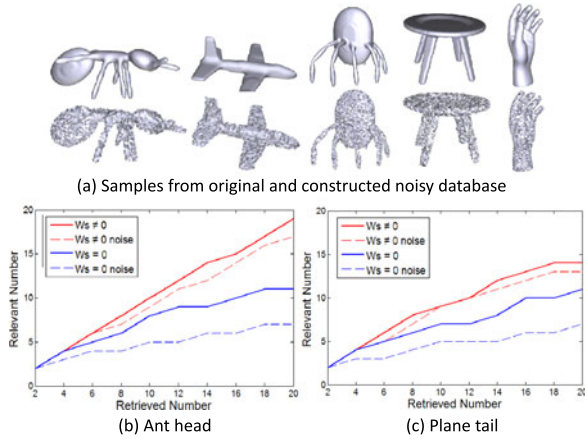


Fig. 10. Retrieval results (on SHREC database) with $w_s = 0$ (red line) and $w_s \neq 0$ (blue line), and dash lines show the results on noisy models.

number of graph wavelets' time scales is set to be 5, which can well represent the frequency information. We empirically set the number of the bins in distance distribution to be 10, and it has been tested to be sufficient to characterize the structure features. The weights ω_s and ω_p are automatically set (based on the mean scale of each part) to balance the three parts that comprise the descriptor. Fig. 10 demonstrates the function of graph wavelets by comparing the retrieval results with $w_s = 0$ and $w_s \neq 0$ on SHREC database and the corresponding constructed database (note that each model is added with 0.5 mean-edge-length noise as shown in Fig. 10a). The relevant number is the number of retrieved models that contain partial regions that match the query region (here, ant head and plane tail). It clearly shows that graph wavelets holds the power to characterize the focus regions discriminatively and robustly. Therefore, we selectively enlarge the weight of SGWs-related part (w_s) to combat the disadvantages of the other parts in specific applications.

Sampling rate. The setting of sampling rate depends on specific applications. Even when the sampling rate is decreased to 5 percent, our sampling strategy still ensure the inclusion of endpoints. It should be noted that if the application requires high-precision detection, all the vertices of the model could be taken into consideration. For the feature detection framework, the sampling rate of 20 percent can meet almost all the needs in our experiments.

Signal selection. The signal function influences SGW-related statistics directly. Therefore, signal selection is among the key problems that should be considered. In principle, the selection depends on specific applications as analyzed in Section 4. Furthermore, some applications require the signal to be intrinsic, for which signals like Gaussian curvature, thickness, etc. are expected to perform better.

6.2 Repetitive Feature Detection within Certain Model

Repetitive feature detection is of great importance to applications, such as self-symmetry detection [20] and non-local processing propagation [27]. We randomly select some regions of interest to be the shape features as illustrated in Fig. 11 (in red). The specified features show that our diffusion-manner demarcation can well cover the interest regions of any kind of shapes if only the interest points and

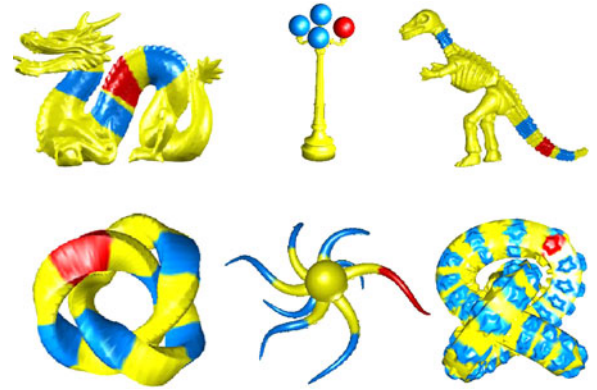


Fig. 11. Repetitive feature detection within certain model. Red denotes query feature and blue denotes some detected results.

scopes are chosen properly. The detection results show that our descriptor can reliably locate the repetitive feature regions within the dragon model even with large deformations, and it can effectively distinguish between the lumpy local shape of dinosaur's tail from its cylinder-like legs, etc. It very well demonstrates that our SGW-centered descriptor can depict the local details and reflect multi-scale geometric distortions thanks to its gradational construction.

6.3 Feature Detection in Database

The performance of our feature detection framework is evaluated on the SHREC 2007 watertight retrieval benchmark, which contains 20 categories and each consists of 20 meshes. In order to demonstrate that our framework is not restricted to the segmentation-based regions like four-legs, we test three kinds of artificial models and each of the query model is unique without any transformed equivalent in the dataset.

We deliberately specify features on kettle, glasses, and chair as shown in Fig. 12a. The slab of the chair is a vivid example, and the existing methods based on segmentation cannot achieve such trans-boundary shapes. It's obvious that the top-4 similar parts in Fig. 12b resemble the query

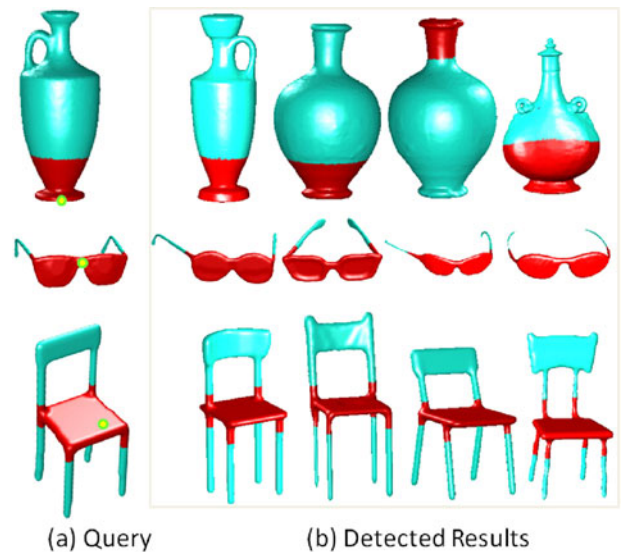


Fig. 12. Feature detection on the SHREC 2007 watertight retrieval database.

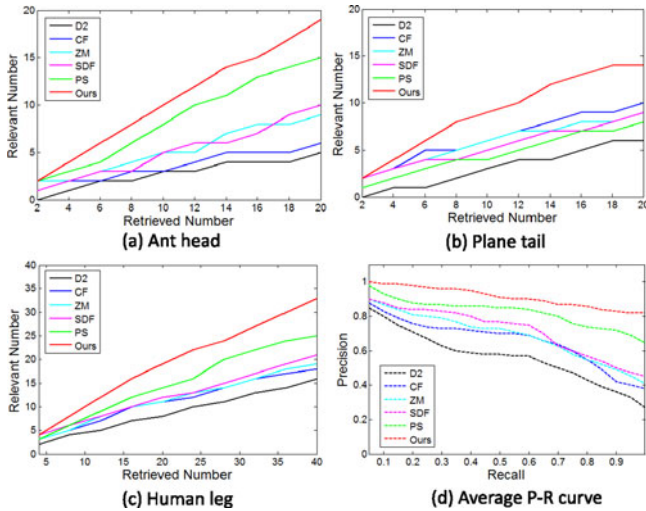


Fig. 13. Precision plots of different detection methods. (a)-(c) show results of different queries. (d) shows the average P-R graph on SHREC watertight database.

region very well, which validates that our descriptor based on the continuously distributed contours could characterize the focal region thoroughly. The feature detection process has the ability to correctly identify the most similar parts with equal-proportional scales thanks to the stable characteristic of bi-harmonic distance. By examining which models in the database contain the similar shapes such as kettle base, eyeglasses or slab of chair, our framework can facilitate co-analysis across models and enable search-based shape modeling.

6.4 Comparisons and Discussion

Due to the unique technical strategy of our feature description and detection, there is no existing work that is directly comparable with ours. From the perspective of applications, partial matching appears to be the most relevant one. Therefore, we first compare our approach with five popular existing methods in partial matching or shape retrieval based on region description. These methods can all properly fit into our framework and make effective comparisons. They are

- D2 Shape Distribution (D2): statistics of distances between any random pair of points on the region [11].
- Conformal Factors (CF): statistics of conformal geometric factors of points on the region [12].
- Zernike Moments based signature (ZM): local shape signature based on transformation of Zernike Moments [27].
- Local SDF Signature (SDF): statistics of points' Shape Diameter Function [25].
- Patch Spectral Geometric Features (PS): normalized spectra of patch spectrum decomposition [14].

The above methods induce the direct geometric measurement (D2), intrinsic curvature-related measurement (CF), heightmap-based measurement (ZM), volume-based measurement (SDF), and spectral-analysis measurement (PS), respectively.

We conduct comparison tests on SHREC 2007 watertight database as well as the McGill database that contains 255

TABLE 2
Precision of Different Detection Methods

Method	Ant Head		Plane Tail		Human Leg	
	15	30	15	30	30	60
Ideal	100%	66.7%	100%	66.7%	100%	66.7%
D2	26.7%	30.0%	26.7%	23.3%	40.0%	41.7%
CF	33.3%	30.0%	53.3%	56.7%	46.7%	48.3%
ZM	53.3%	43.3%	53.3%	53.3%	46.7%	50.0%
SDF	46.7%	56.7%	46.7%	50.0%	50.0%	58.3%
PS	80.0%	60.0%	46.7%	43.3%	73.3%	60.0%
Ours	93.3%	63.3%	80.0%	60.0%	86.7%	63.3%

objects divided into ten classes and the intra-class variations consist of non-rigid transforms applied to models. By setting proper parameters in the above methods, effective results are achieved. Fig. 13 shows the detection results of all methods concerned. (a)-(c) are the detection results with the queries of ant head, plane tail, and human leg. In the SHREC database, every category contains 20 different models, so we retrieve the top 20 results of ant head and 40 for human leg, since left and right legs of human are documented separately (we call it the multiple-region case). (d) shows the average PR graph based on all queries without multiple regions.

Table 2 details the precisions of different detection methods. The precision is computed as the ratio of relevant number to the retrieved number (the second line shows the retrieved number for each query). Table 2 and Fig. 14 collectively show that each method has its own strength in describing some specific kind of shape. D2 is excellent in describing regular shapes, such as spheres, because the histogram statistics sometimes have the averaging effect on the spatial information, and the ant head with two tentacles makes it difficult for D2 to depict. CF, which integrates the gaussian-curvature knowledge, performs well in characterizing highly-curved region such as the plane tails. ZM is suitable for depicting small patches, as for large feature regions it works better in detecting highly curved ones. SDF takes into account the volume-based information and the region's area ratio knowledge, so it performs well for cylinder-like shape, but not for local complex shapes. PS performs very well in most cases except for the relatively small and complex structure like plane tails due to the instability of regional Laplacian decomposition. In contrast, our method performs stably with high precision in detecting various types of feature regions across different models.

Moreover, we conduct the comparison with two most related works that cannot fit into our feature detection framework, namely, Gal's [20] and Itskovich's works [21]. Since these two works obtain the feature regions by decomposition process and clustering of the pre-divided patches, there inevitably exist over-segmentation phenomenon as shown in the zoomed-in part of Fig. 15. In comparison, our method can flexibly specify the interesting feature region and exactly detect the similar regions with the proper scales.

6.5 Applications

Our feature detection framework enjoys plenty of desirable properties as demonstrated in Section 5. They can further

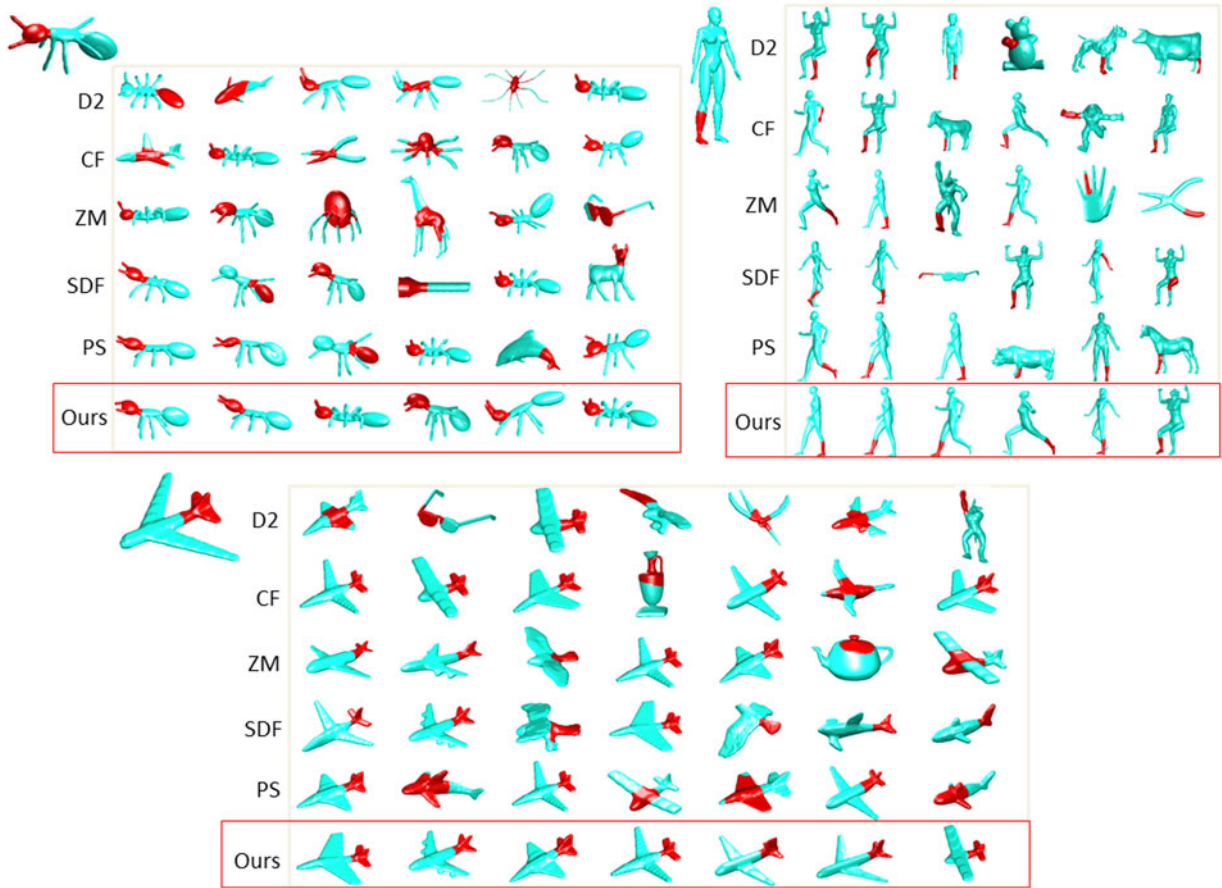


Fig. 14. Comparison of different detection methods for partial matching. The queries are ant head, human leg, and plane tail.

facilitate a host of applications as will be shown and analyzed.

Partial matching and restoration. We analyze the combined models from SHREC 2007’s partial retrieval dataset, which comprises the SHREC 2007’s watertight dataset and a query set of 30 models. Each combined model is obtained by merging or removing several subparts of models belonging to the watertight dataset. Existing algorithms concerning partial matching consider the retrieval of the query set

models as a big challenge. We demonstrate that our framework provides a powerful tool to restore the combined models, thus can effectively aid the matching and recognition. As the three cases shown in Fig. 16, choosing proper interest points (yellow points in (a)) and contour scopes could give rise to diffusion regions that cover large scale of the searched models. After completing the detecting process in the watertight database, the original model can be

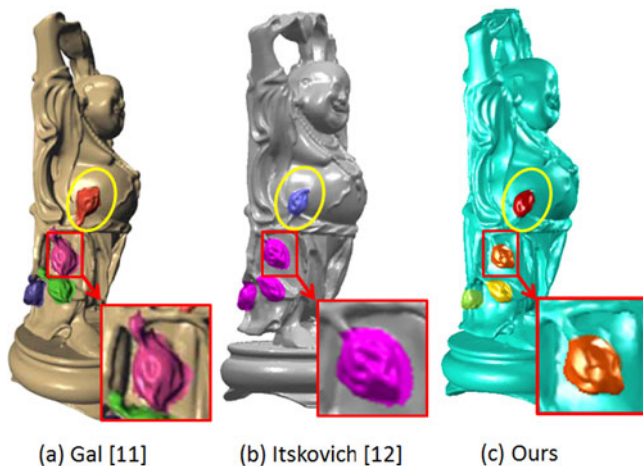


Fig. 15. Comparison on detection of complex feature regions. Figure (a) and (b) are cited from the corresponding works. On each model, the flower inside the yellow circle is the query region.

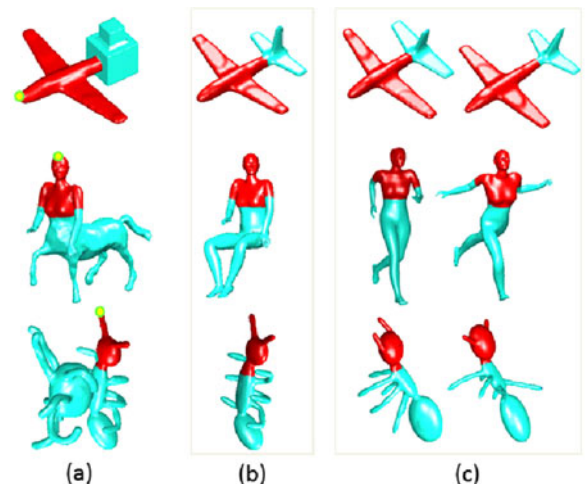


Fig. 16. Partial matching and restoration on the SHREC’s partial query dataset. (a) Combined models with query regions in red. (b) Restored models. (c) Another two models containing the top-ranked similar feature regions.

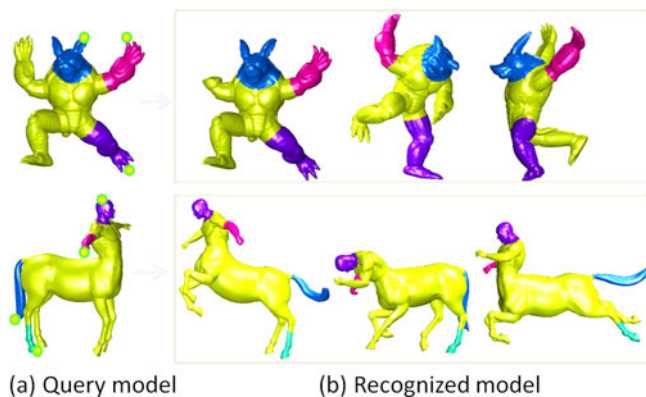


Fig. 17. Model recognition by identifying multiple components of current interest. (a) Query models with 3 or 4 specified features. (b) Top-3 recognized models.

recognized as shown in (b), and (c) shows another two detected models containing the top-ranked similar feature regions. Moreover, if conventional point-wise correspondence is required for downstream tasks, we can further achieve this goal easily. Since our feature is defined in a diffusion manner, after the similar region is matched, the exact point matching can be obtained by shrinking the diffusion region back to its source point, thus helping the conventional point-based correspondence and other complex partial matching tasks.

Model recognition. Another immediate application is model recognition based on key components as suggested in [6]. The feature detection framework is much more powerful and does not need the complex process of finding key components as in [6]. Fig. 17a shows the query models, on which we selectively specify three or four features that are considered to be essential for characterizing the armadillo and horse model. The whole shape similarity is computed as the sum of the distances between the specified feature regions of the query model and the corresponding regions of the target model. Apparently, specifying more feature regions can achieve more precise results. The ranked retrieval results in Fig. 17 b show that our method can correctly retrieve the relevant models from the database even when the models are somewhat incomplete (like the first recognized armadillo model).

Other potential applications. Many more practical applications could potentially benefit from the attractive properties of our approach. For example, thanks to the robustness demonstrated in Section 5, our framework can serve as the foundation for search-based modeling and coarse-to-fine part replacement that frequently relies upon the conventional denoising processes in the pre-processing stage. The reliability demonstrated in the test of repetitive feature detection shows that our detection results could potentially help with the recognition of repeated patterns, cut-and-paste editing, and self-symmetry detection. Since the technical foci of this paper is to build the theoretical foundation for our feature description and demonstrate its effectiveness via the core applications of feature detection, we could not do a full justice to cover numerous other applications (due to paper's page limit). Our future work shall try to broaden the framework's application scope.

Limitation. Our feature detection framework is built upon bi-harmonic distance field, and the boundaries of features in the approach are defined using the contours, which may not depict regions confined by arbitrary curved boundaries. Another limitation is that our approach may have difficulties in dealing with model defects, such as the existence of big holes or missing large organic parts. These will be the topics for our future research.

7 CONCLUSION AND FUTURE WORK

In this paper we have detailed the description and detection of our proposed generalized local-to-global features on 3D geometric models, which organically couple both local (differential) and global (integral) geometric attributes. The multi-scale and multi-level descriptor based on SGWs has exhibited its potential in depicting any user-specified feature region and distinguishing among descriptor vectors in the corresponding region-wise descriptor space. Furthermore, our novel descriptor is comprising many desirable properties which can facilitate a host of graphics applications, as showcased in our comprehensive experiments. Extensive comparisons with other state-of-the-art techniques/methods have demonstrated certain key advantages of our method in terms of geometry-awareness, reliability, robustness, etc.

Our future work will try to make the interface's functionality more flexible and intuitive, allowing users to sketch the boundary of any intended feature region. We plan to incorporate more powerful analytical tools into our descriptor space for various kinds of analysis. We also intend to broaden the application scope of the proposed shape features to support feature-centric registration, structure-driven co-segmentation, and high-fidelity model production.

ACKNOWLEDGMENTS

The authors wish to thank all the reviewers for their valuable comments. This work is partially supported by the National Natural Science Foundation of China grants (61300083, 61432003, 61173103, 91230103, 61320106008, 61532002, 61190120, 61190121, 61190125), and the US National Science Foundation grants IIS-(0949467, 1047715, 1049448).

REFERENCES

- [1] A. M. Bronstein, M. M. Bronstein, L. J. Guibas, and M. Ovsjanikov, "Shape google: Geometric words and expressions for invariant shape retrieval," *ACM Trans. Graph.*, vol. 30, no. 1, pp. 1–20, 2011.
- [2] O. Kin-Chung Au, Y. Zheng, M. Chen, P. Xu, and C.-L. Tai, "Mesh segmentation with Concavity-aware fields," *IEEE Trans. Vis. Comput. Graph.*, vol. 18, no. 7, pp. 1125–1134, Jul. 2012.
- [3] R. Song, Y. Liu, R. R. Martin, and P. L. Rosin, "Mesh saliency via spectral processing," *ACM Trans. Graph.*, vol. 33, no. 1, pp. 1–17, 2014.
- [4] T. Funkhouser, M. Kazhdan, P. Shilane, P. Min, W. Kiefer, A. Tal, S. Rusinkiewicz, and D. Dobkin, "Modeling by example," *ACM Trans. Graph.*, vol. 23, no. 3, pp. 652–663, 2004.
- [5] V. Kreevov, D. Julius, and A. Sheffer, "Model composition from interchangeable components," in *Proc. Pacific Conf. Comput. Graph. Appl.*, 2007, pp. 129–138.
- [6] I. Sipiran and B. Bustos, "Key-component detection on 3D meshes using local features," in *Proc. 5th Eur. Conf. 3D Object Retrieval*, 2012, pp. 25–32.

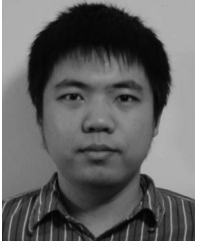
- [7] M. Kazhdan, T. Funkhouser, and S. Rusinkiewicz, "Rotation invariant spherical harmonic representation of 3D shape descriptors," in *Proc. ACM Symp. Geometry Process.*, 2003, pp. 156–164.
- [8] M. Mortara, G. Patané, M. Spagnuolo, B. Falcidieno, and J. Rossignac, "Blowing bubbles for the Multi-scale analysis and decomposition of Triangle-meshes," *Algorithmica*, vol. 38, no. 1, pp. 227–248, 2003.
- [9] T. Gatzke, C. Grimm, M. Garland, and S. Zelinka, "Curvature maps for local shape comparison," in *Proc. Int. Conf. Shape Model. Appl.*, 2005, pp. 244–253.
- [10] I. Kokkinos, M. Bronstein, R. Litman, and A. Bronstein, "Intrinsic shape context descriptors for deformable shapes," in *Proc. IEEE Comput. Vis. Pattern Recog.*, 2012, pp. 159–166.
- [11] R. Osada, T. Funkhouser, B. Chazelle, and D. Dobkin, "Shape distributions," *ACM Trans. Graph.*, vol. 21, no. 4, pp. 807–832, 2002.
- [12] M. Ben-Chen and C. Gotsman, "Characterizing shape using conformal factors," in *Proc. 1st Eurographics Conf. 3D Object Retrieval*, 2008, pp. 1–8.
- [13] Y. Liu, H. Zha, and H. Qin, "Shape topics: A compact representation and new algorithms for 3D partial shape retrieval," in *IEEE Comput. Vis. Pattern Recog.*, 2006, pp. 2025–2032.
- [14] J. Hu and J. Hua, "Salient spectral geometric features for shape matching and retrieval," *Vis. Comput. Int. J. Comput. Graph.*, vol. 25, nos. 5–7, pp. 667–675, 2009.
- [15] G. Lavoué, "Combination of Bag-of-words descriptors for robust partial shape retrieval," *Vis. Comput.*, vol. 28, no. 9, pp. 931–942, 2012.
- [16] Y. Lamdan and H. J. Wolfson, "Geometric hashing: A general and efficient Model-based recognition scheme," in *Proc. 2nd Int. Conf. Comput. Vis.*, 1988, pp. 238–249.
- [17] M. Fischler, R. Bolles, A. Varshney, and R. Farias, "Random sample consensus: A paradigm for model fitting with applications to image analysis and automated cartography," *Commun. ACM*, vol. 24, no. 6, pp. 381–395, 1981.
- [18] R. M. Rustamov, "Multiscale biharmonic kernels," *Comput. Graph. Forum*, vol. 30, no. 5, pp. 1521–1531, 2011.
- [19] J. Sun, M. Ovsjanikov, and L. Guibas, "A concise and provably informative Multi-scale signature based on heat diffusion," in *Proc. Symp. Geometry Process.*, 2009, pp. 1383–1392.
- [20] R. Gal and D. Cohen-Or, "Salient geometric features for partial shape matching and similarity," *ACM Trans. Graph.*, vol. 25, no. 1, pp. 130–150, 2006.
- [21] A. Itskovich and A. Tal, "Surface partial matching and application to archaeology," *Comput. Graph.*, vol. 35, no. 2, pp. 334–341, 2011.
- [22] S. Zelinka and M. Garland, "Similarity-based surface modelling using geodesic fans," in *Proc. Eurographics Symp. Geometry Process.*, 2004, pp. 209–218.
- [23] G. Lavoué, "Bag of words and local spectral descriptor for 3D partial shape retrieval," in *Proc. Eurographics Conf. 3D Object Retrieval*, 2011, pp. 41–48.
- [24] R. Toldo, U. Castellani, and A. Fusiello, "Visual vocabulary signature for 3D object retrieval and partial matching," in *Proc. 2nd Eurographics Conf. 3D Object Retrieval*, 2009, pp. 21–28.
- [25] L. Shapira, S. Shalom, A. Shamir, D. Cohen-Or, and H. Zhang, "Contextual part analogies in 3D objects," *Int. J. Comput. Vis.*, vol. 89, nos. 2/3, pp. 309–326, 2010.
- [26] J. Pokrass, A. M. Bronstein, and M. M. Bronstein, "Partial shape matching without Point-wise correspondence," *Numerical Math.*, vol. 6, no. 1, pp. 223–244, 2013.
- [27] A. Maximo, R. Patro, A. Varshney, and R. Farias, "A robust and rotationally invariant local surface descriptor with applications to Non-local mesh processing," *Graph. Models*, vol. 73, no. 5, pp. 231–242, 2011.
- [28] L. Jiang, X. Zhang, and G. Zhang, "Partial shape matching of 3D models based on the Laplace-beltrami operator eigenfunction," *J. Multimedia*, vol. 8, no. 6, pp. 655–661, 2013.
- [29] S. Biasotti and S. Marini, "Sub-part correspondence using structure and geometry," in *Proc. Eurographics Italian Chapter Conf.*, 2006, pp. 23–28.
- [30] A. M. Bronstein and M. M. Bronstein, "Regularized partial matching of rigid shapes," in *Proc. Eur. Conf. Comput. Vis.*, 2008, pp. 143–154.
- [31] U. Castellani, M. Cristani, S. Fantoni, and V. Murino, "Sparse points matching by combining 3D mesh saliency with statistical descriptors," *Comput. Graph. Forum*, vol. 27, no. 2, pp. 643–652, 2008.
- [32] A. Zaharescu, E. Boyer, K. Varanasi, and R. Horaud, "Surface feature detection and description with applications to mesh matching," in *IEEE Comput. Vis. Pattern Recog.*, 2009, pp. 373–380.
- [33] M. Bronstein and I. Kokkinos, "Scale-invariant heat kernel signatures for non-rigid shape recognition," in *Proc. IEEE Comput. Vis. Pattern Recog.*, 2010, pp. 1704–1711.
- [34] S. Mallat, *A Wavelet Tour of Signal Processing, Third Edition: The Sparse Way*. San Francisco, CA, USA: Academic, 2008.
- [35] N. Werghi and Y. Xiao, "Wavelet moments for recognizing human body posture from 3D scans," in *Proc. Int. Conf. Pattern Recog.*, 2002, pp. 319–322.
- [36] Z. Liu, J. Mitani, Y. Fukui, and S. Nishihara, "A 3D shape retrieval method based on continuous spherical wavelet transform," in *Proc. Int. Conf. Comput. Graph. Imag.*, 2007, pp. 21–26.
- [37] R. Coifman and S. Lafon, "Diffusion maps," *Appl. Comput. Harmonic Anal. Diffusion Maps Wavelets*, vol. 21, no. 1, pp. 5–30, 2006.
- [38] T. Hou and H. Qin, "Admissible diffusion wavelets and their applications in space-frequency processing," *IEEE Trans. Vis. Comput. Graph.*, vol. 19, no. 1, pp. 3–15, Jan. 2013.
- [39] D. Hammond, P. Vandergheynst, and R. Gribonval, "Wavelets on graphs via spectral graph theory," *Appl. Comput. Harmonic Anal.*, vol. 30, no. 2, pp. 129–150, 2011.
- [40] T. Hou and H. Qin, "Continuous and discrete mexican hat wavelet transforms on manifolds," *Graphical Models*, vol. 74, no. 4, pp. 221–232, 2012.
- [41] W. H. Kim, M. K. Chung, and V. Singh, "Multi-resolution shape analysis via Non-euclidean wavelets: Applications to mesh segmentation and surface alignment problems," in *Proc. IEEE Comput. Vis. Pattern Recog.*, 2013, pp. 2139–2146.
- [42] W. H. Kim, V. Singh, M. K. Chung, C. Hinrichsa, and D. Pachauri, "Multi-resolutional shape features via Non-euclidean wavelets: Applications to statistical analysis of cortical thickness," *Neuro-Image*, vol. 93, no. 1, pp. 107–123, 2014.
- [43] C. Li and A. Ben Hamza, "A multiresolution descriptor for deformable 3D shape retrieval," *Vis. Comput.*, vol. 29, no. 6–8, pp. 513–524, 2013.
- [44] Y. Lipman, R. M. Rustamov, and T. A. Funkhouser, "Biharmonic distance," *ACM Trans. Graph.*, vol. 29, no. 3, pp. 1–11, 2010.
- [45] M. Meyer, M. Desbrun, P. Schröder, and A. Barr, "Discrete differential-geometry operators for triangulated 2-manifolds," in *Visualization and Mathematics III*. Berlin, Germany: Springer, 2003, pp. 35–57.
- [46] C. Moenning and N. A. Dodgson, "Fast marching farthest point sampling for point clouds and implicit surfaces," Cambridge Univ., Cambridge, U.K., Tech. Rep. 565, 2003.



Nannan Li received the BS degree in applied mathematics from Dalian University of Technology in 2010. She is a PhD degree candidate in School of Mathematical Sciences at Dalian University of Technology. Her research interests include computer graphics, differential geometry processing and analysis, and machine learning.



Shengfa Wang received the BS and PhD degrees in computational mathematics from Dalian University of Technology. He is a lecturer in the School of Software Technology and Key Laboratory for Ubiquitous Network and Service Software of Liaoning Province at Dalian University of Technology. His research interests include computer graphics, diffusion geometry, and differential geometry processing and analysis.



Ming Zhong received the BEng degree from University of Science and Technology of China in 2010. He is a PhD degree candidate in the Department of Computer Science, Stony Brook University. His research interests include geometric modeling and processing, shape correspondence, and computer vision.



Zhixun Su received the BS degree in mathematics from Jilin University, MS degree in Computer Science from Nankai University and the PhD degree in computational mathematics from Dalian University of Technology. He is a professor in the School of Mathematical Sciences and the director in the Key Lab of Computational Geometry, Graphics and Images at Dalian University of Technology and National Engineering Research Center of Digital Life in Guangzhou. His research interests include on computational geometry, computer graphics, image processing, and computer vision.



Hong Qin received the BS and MS degrees in computer science from Peking University, China. He received the PhD degree in computer science from the University of Toronto. He is a full professor of computer science in the Department of Computer Science at Stony Brook University (SUNY Stony Brook). He is currently serves as an associate editor for *The Visual Computer*, *Graphical Models*, and *Journal of Computer Science and Technology*. His research interests include geometric and solid modeling, graphics, physics-based modeling and simulation, computer aided geometric design, human-computer interaction, visualization, and scientific computing. He is a senior member of the IEEE.

▷ **For more information on this or any other computing topic, please visit our Digital Library at www.computer.org/publications/dlib.**